The Role of Sm^{3+} Energy Transfer on White Emission of $La_{1.98}Dy_{0.02}MgTiO_6$ Double Perovskite Nano-Phosphors for Endoscopy and Laparoscopy LEDs

Vannadil Puthiyaveetil Veena, Cherlan Kottianmadathil Shilpa, Seere Valappil Jasira, and Kavukuzhi Meerasahib Nissamudeen*

School of Pure and Applied Physics, Kannur University, Payyanur, Kannur district, Kerala 670327, India

***e-mail:** nisamkm@kannuruniv.ac.in

Abstract. Decent lighting is a major requisite in Laparoscopic and Endoscopic examinations, as the illumination is below the edge value, the image becomes distorted resulting inaccurate outcome. Double perovskites with flexible formulas and structures, lithic chemical-physical properties, and suitable optical bandgap, are the most suited candidates for such illumination devices. Novel perovskite nano-phosphor $La_{1.97}Dy_{0.02}Sm_{0.01}MgTiO_6$ ace among the group with violet-blue-yellow-red emission, which gives luminescence 3-fold than conventional lighting sources, owing to $Dy^{3+}\rightarrow Sm^{3+}$ energy transfer mechanism with efficiency 53%. The Commission Internationale de I'Elcairage (CIE) chromaticity coordinates are (0.322, 0.324) with color temperature 5835K, neighboring to ideal white light, which is threshold in picking the exact light source for endoscopic and laparoscopic applications. So, a meticulous optimization on broad white emission of $La_{1.97}Dy_{0.02}Sm_{0.01}MgTiO_6$ to the neutral point for biomedical application is an inevitability.

Keywords: perovskite nano-phosphors, endoscopy, white light emitting diodes.

Paper #7649 received 22 Feb 2023; revised manuscript received 4 Jul 2023; accepted for publication 8 Jul 2023; published online 14 Aug 2023. doi: 10.18287/JBPE23.09.030307.

1 Introduction

The advent of a fast-growing field, nanotechnology has made a great leap in energy, environment, and healthcare zones. Nanoscience and nanotechnology deal with the control of matter on an atomic or molecular scale. This knowledge fostered human life much simpler and easier. At this point, nano-medicines, nano-devices, and nano-probes have revolved around a healthy environment for balanced health requirements. The use cases range from drug delivery to tissue engineering, biosensors, and diagnostics. Human health and total well-being are central to economic growth [1]. So, the early detection and treatment of infirmity are crucial for human prosperity, which can be achieved through precise instrumentation setups. Biomedical engineering is advancing copiously in improving the healthcare sector with high-resolution real-time image recording devices that could improve disease detection and treatment probability. As the patient experiences minimal suffering and undergoes fast recovery, minimal invasive surgery (MIS) by means of endoscopes and laparoscopes, aids human well-being to a prodigious extent. The light source plays a vital role at this time in disease identification and examination. That is, good illumination is a major requisite in MIS treatment, as the intensity level is below the threshold value, the image gets distorted [2]. That is, the endoscopic examination involves real-time internal tissue imaging using a device equipped with a CCD camera attached to a high-brightness ideal light source. As the internal tissues are away from our line of sight, this device is inserted through the mouth, inside the body through the esophagus, duodenum, and stomach. Once it reaches the target site, using the CCD camera, the tissue is subjected to imaging and inspection (Fig. 1) [3]. The practicing xenon arc lamps grieve plasma oscillations and thermal runaway, leading to instability. At the same time, the UV radiations given out by them are prone to skin and cause damages to eye structure [4].

This paper was presented at the International Conference on Nanoscience and Photonics for Medical Applications – ICNPMA, December 28–30, 2022, Manipal, India.

Table 1 Comparison of properties of conventional xenon arc lamp and white LED (wLED).

Conventional Xenon arc lamp	wLEDs
Suffer plasma oscillations and thermal runaway	Minimal energy consumption, high efficiency, good brightness, longer operation time
The UV radiations are prone to skin and causes injury to eye structure	Eco-friendly in nature
Costly and require replacement after every 500 h run	Lifetime about 50,000 h
Violet spectral region is present	Violet spectral region is absent
Wide range emission	Fabricated by combining red-green-blue LEDs or by coating yellow phosphor on blue LED

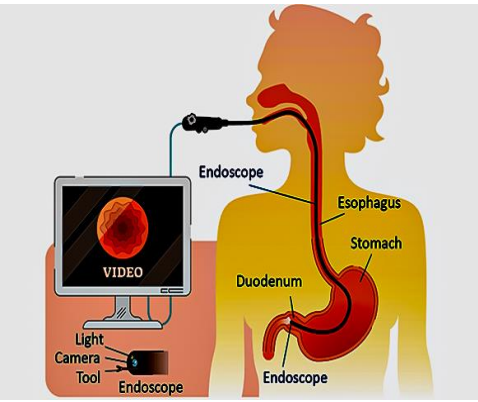

Fig. 1 Endoscopy procedure.

These lamps are expensive and involve a replacement after every 500 h of usage (Table 1). Recently, a white LED (wLED) source with a lifetime of about 50,000 h is swapping traditional arc lamps. However, the chief bottleneck lies is the lack of violet spectral region, which is inevitable in determining diseases [3, 5] like lesions, patterns of colonic mucosa, and adenoma (polyp) tumors [6].

The lighting sector is striving hard to replace conventional imaging sources of the health sector with an environmentally friendly, abiding, flexible, energy-saving, efficient, and miniature arrangement, that could improve the eminence of real-time recorded data. The double perovskite nano phosphors are among the group that is gaining ample attention in luminescence nanoscience research, owing to their wide applications in domestic, industrial, commercial, and health sectors [7–10]. The fourth-generation illumination technology, phosphor-converted white light emitting devices (wLED), that convert excitation energy to ideal visible white light flags this demand. Topical rummages suggest that the perovskite structure has been found to have very low toxicity and is truly biocompatible with human cells.

The potential double perovskite host matrix La_2MgTiO_6 ($A_2BB^{|}O_6$) is attaining much research fascination at this instant due to its unique luminescence properties when doped with apt rare earth ions [7, 11]. Dysprosium ions are doped in the crystal lattice of La_2MgTiO_6 perovskite nano-phosphors, co-activated by Samarium ions. The photoluminescence spectra reveal that the $La_{1.97}Dy_{0.02}Sm_{0.01}MgTiO_6$ emanate violet-blue-yellow-red emission peaks at 388 nm, 480 nm, 574 nm, and 670 nm corresponding to $^4F_{7/2} \rightarrow {}^6H_{15/2}$, $^4F_{9/2} \rightarrow {}^6H_{15/2}$, $^4F_{9/2} \rightarrow {}^6H_{13/2}$ and $^4F_{9/2} \rightarrow {}^6H_{11/2}$ transitions respectively [8–10]. This violet emission, which is generally absent in existing white LEDs, is of great importance in the health sector, mainly in identifying infirmities like polyps. The Commission Internationale de I'Elcairage (CIE) chromaticity of $La_{1.97}Dy_{0.02}Sm_{0.01}MgTiO_6$ is very close to ideal white light with luminescence intensity two times higher than that of commercially available wLED YAG:Ce^{3+}. So, an ideal white emitting source with violet spectral component is a necessity to boost the health sector.

2 Materials and Methods

Perovskite nano-phosphor $La_{1.97}Dy_{0.02}Sm_{0.01}MgTiO_6$ is prepared by combustion method. Quantitative ratios of analytical grade La_2O_3, MgO, TiO_2, Dy_2O_3 and Sm_2O_3 are constantly heated and stirred in 8 M HNO_3, unless it reduces to 40%. 1:2 ratio of citric acid is added as the fuel. When it makes a gel form, the mix is transferred to a corundum crucible and ignited in a muffle furnace at 1223 K for 4 h. After gradual cooling, the perovskite is powdered well, without any lumps. Using Rigaku, Smartlab X-ray diffractometer, the crystal structure and phase is investigated. The powder morphology, crystallinity, and shape were examined by field emission scanning electron microscopy (FE-SEM, ZEISS) and transmission electron microscopy (TEM, JEM-2100 Plus). The Flurolog, Horiba photoluminescence spectrometer is castoff for emission studies.

3 Results and Discussion

The X-ray diffraction (XRD) pattern of synthesized $La_{1.97}Dy_{0.02}Sm_{0.01}MgTiO_6$ perovskite nano-phosphor is indexed with standard ICDD card – 86852 and found to crystallize in orthorhombic crystal structure with space group *pbnm* (Fig. 2). The A site of the perovskite is occupied by La^{3+}, Dy^{3+} and Sm^{3+} ions. The B, $B^{|}$ sites are occupied by Mg^{2+} and Ti^{4+} respectively. Dy^{3+} and Sm^{3+} doping makes no noticeable changes in the La_2MgTiO_6 crystal frame.

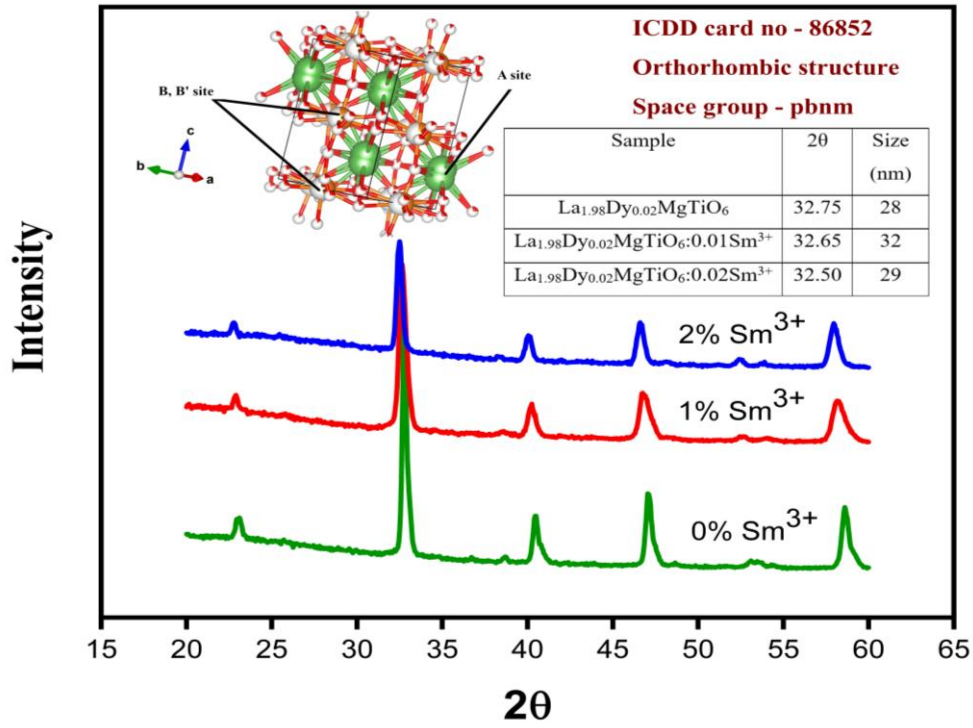

Fig. 2 XRD pattern of $La_{1.97}Dy_{0.02}Sm_{0.01}MgTiO_6$.

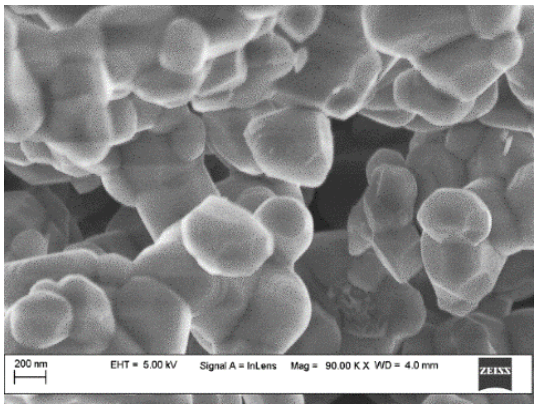

(a)

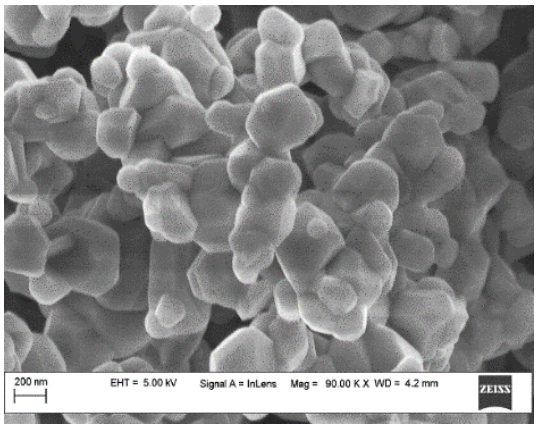

(b)

Fig. 3 FE-SEM images before Sm^{3+} co-doping (a) and after Sm^{3+} co-doping (b).

Due to the similar ionic radius, Dy^{3+} and Sm^{3+} are infixed in the La^{3+} crystal lattice. No additional peaks are observed, which ensure that Dy^{3+} and Sm^{3+} ions are well lodged in the host lattice from the XRD data, the particle size is calculated using Debye Scherrer Eq.:

$$D = \frac{k\lambda}{\beta cos\theta}, \quad (1)$$

where $k = 0.99$ is the shape factor, θ is the diffraction angle, λ is the wavelength of X-ray, and β is the full width at half maximum of the major peak (FWHM) [11], δ the dislocation density of $La_{1.97}Dy_{0.02}Sm_{0.01}MgTiO_6$ is calculated as $\delta = \frac{1}{D^2} = 0.00096$ nm^{-2}, which is negligible and is congruent with XRD pattern. The lattice strain (ε) is of the order of 0.003×10^{-3}, which can also be neglected [8]. The major peaks are sharp and pointed with broader noticeable FWHM, indicating the formation of nano-powders with crystalline environment [12]. The decrease in crystallinity with doping is due to lattice distortion [13], depending on the relative ionic radii of dopant and host site. Since the radii percentage difference of Dy^{3+} and Sm^{3+} is 5% (x<<35%), the deformation is minimum and thus acceptable. The crystal size, structure and morphology are confirmed using FE-SEM and TEM (Figs. 3, 4). It is evident that the perovskite phosphors are nano-sized crystalline particles that agglomerate to form a cauliflower like structure. Following the XRD and SEM and TEM images, it is evident that the crystallinity of the samples decreases with increase in Sm^{3+} concentration. It can be attributed to the increase in deformation of the crystal lattice due to the external doping.

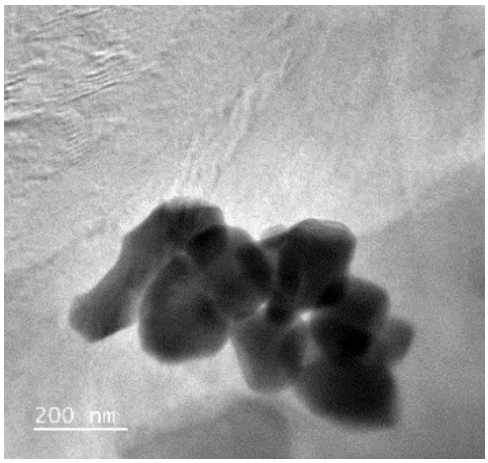

(a)

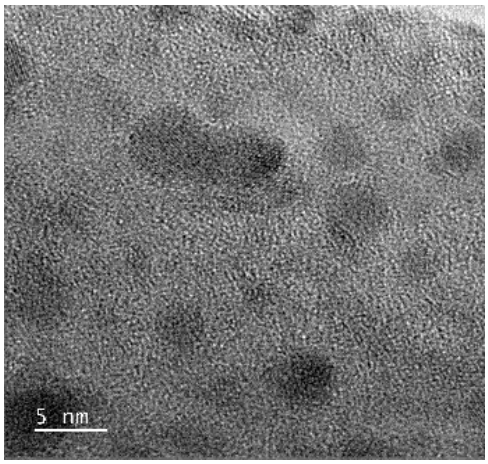

(b)

Fig. 4 TEM images after Sm^{3+} co-doping (a) 200 nm and (b) 5 nm resolution.

The photoluminescence (PL) studies are carried out using spectrophotometer Flurolog, monitored under 351 nm excitation (Fig. 5a). The emission spectra show four prominent peaks violet, blue, yellow, and red owing to different energy transition levels of Dy^{3+} ion. That is, emission peaks at 388 nm (violet), 480 nm (blue), 574 nm (yellow), and 670 nm (red) agreeing to $^4F_{7/2} \rightarrow {}^6H_{15/2}$, $^4F_{9/2} \rightarrow {}^6H_{15/2}$, $^4F_{9/2} \rightarrow {}^6H_{13/2}$ and $^4F_{9/2} \rightarrow {}^6H_{11/2}$ transitions [8–10] (Fig. 5b). The lower wavelengths (388 nm and 480 nm) are vulnerable to crystal environment whereas, the higher wavelengths (574 nm and 670 nm) are independent to crystal atmosphere [14–17]. An intense yellow emission is highly favored for white light emitting diodes, which is well observed in $La_{1.97}Dy_{0.02}Sm_{0.01}MgTiO_6$ nano-phosphors. Owing to the overlap between the excitation band of $Sm^{3+}$and emission band of Dy^{3+}, efficient energy transfer occurs between them, resulting the merging of Sm^{3+} ions enhancing the luminescence intensity. As the $^4G_{5/2}$ level of Sm^{3+} possesses orange-red luminescence with a higher lifetime, Sm^{3+} co-activation enhances the luminescence performance of Dy^{3+} triggered perovskites matrices to a noticeable extent. Sm^{3+} concentration is varied in each set (x = 0%, 1%, 2%) and is optimized for 1%, above which concentration quenching is observed [8, 17–18]. The intense peaks are showing ruptures due to crystal field splitting, showing the noble luminescence intensity. The increase in luminescence intensity can also be attributed to the $Dy^{3+} \rightarrow Sm^{3+}$ energy transfer mechanism. The maximum energy transfer efficiency is calculated to be 53% for 1% Sm^{3+} co-activation, using the relation Energy transfer efficiency,

$$\eta = 1 - \frac{I_{Dy}}{I_{Dy \rightarrow Sm}} = 53\%, \qquad (2)$$

where I_{Dy} is the luminescence intensity in Dy^{3+} doped samples and $I_{Dy \rightarrow Sm}$ is the luminescence intensity of Dy^{3+} doped samples with Sm^{3+} co-activation [19, 20]. The peak at 388nm, which is normally absent in conventional wLED, is of great importance in endoscope devices.

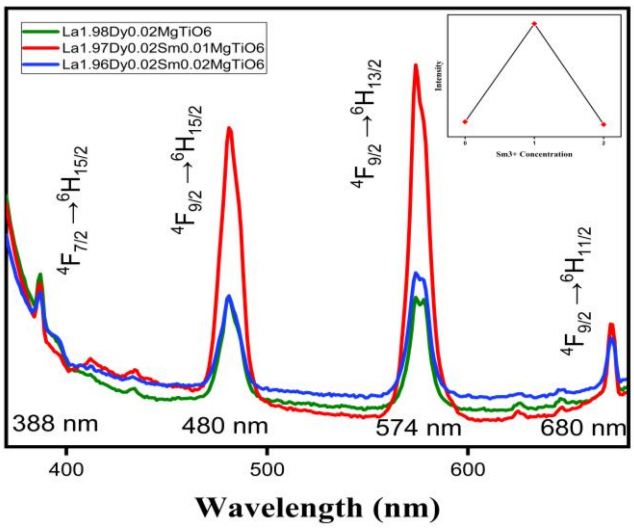

(a)

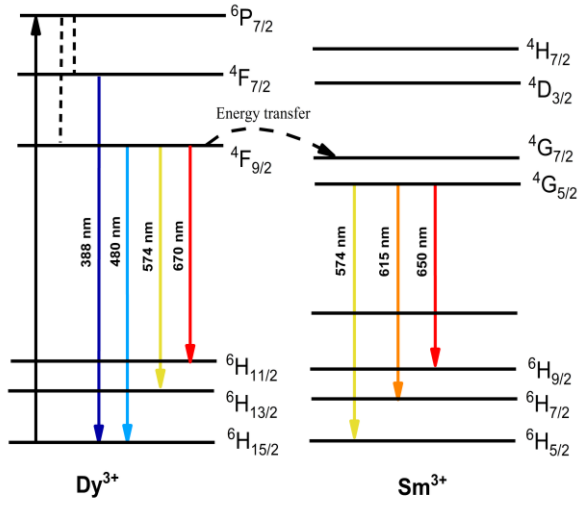

(b)

Fig. 5 (a) Photoluminescence spectra of Sm^{3+} activated samples. (b) $Dy^{3+} \rightarrow Sm^{3+}$ energy transfer mechanism.

Table 2 CIEL*a*b* parameters.

Color	L*	a*	b*	h*	C*	ΔE*
R1	62.0300	12.8136	12.9732	45.3545	18.2343	5.1956
R2	61.3044	−0.4141	30.1181	90.7877	30.1209	1.7179
R3	61.8845	−15.5404	44.0787	109.4206	46.7379	4.2023
R4	60.1403	−25.3198	13.8408	151.3372	28.8558	7.9601
R5	61.6243	−13.2351	−10.2461	217.7457	16.7377	4.9815
R6	60.3764	0.2935	−29.9818	270.5608	29.9832	2.4535
R7	60.6236	16.4615	−24.6955	303.6865	29.6791	3.0057
R8	62.2842	21.9746	−13.7657	327.9354	25.9302	5.4903

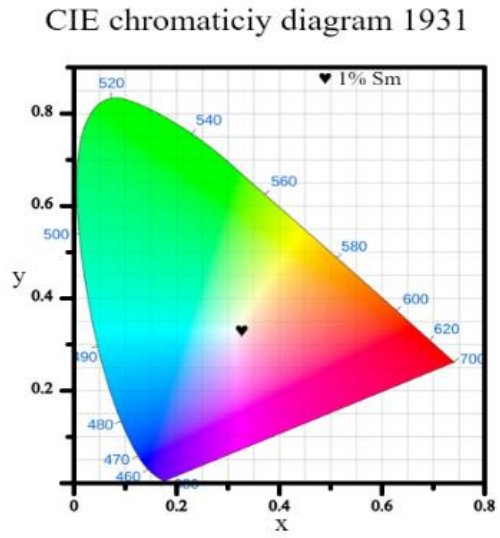

(a)

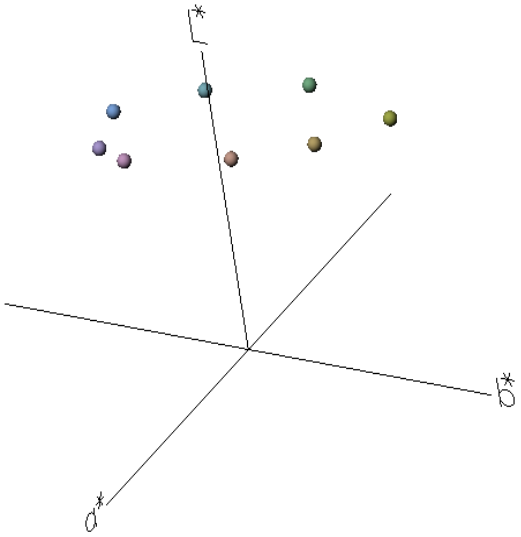

(b)

Fig. 6 (a) CIE chromaticity diagram, (b) CIEL*a*b* colour space.

This spectral region due to $^4F_{7/2} \rightarrow {}^6H_{15/2}$ electronic transition is acute in determining conditions like lesions, patterns of colonic mucosa, and adenoma (polyp) tumors [3, 5–6]. Presence of this violet region makes $La_{1.97}Dy_{0.02}Sm_{0.01}MgTiO_6$ a potential candidate for endoscope LEDs. Moreover, the CIE chromaticity diagram (Fig. 6.a) show color coordinates X = 0.322 and Y = 0.324, is in the neighborhood of ideal white light. The calculated color temperature (CCT) of $La_{1.97}Dy_{0.02}Sm_{0.01}MgTiO_6$ is 5835 K, which is very close to natural sunlight (5900 K). The CCT value, which is a measure of how yellow or blue the emitted light is. That is, CCT above 6500 K is take 'warm' whereas below 4000 K is 'cold' [8]. The color purity is 3.1%, estimated by

$$\text{Color Purity} = \sqrt{\frac{(x-x_i)^2+(y-y_i)^2}{(x-x_d)^2+(y-y_d)^2}} \times 100\%, \qquad (3)$$

where (x, y), (x_i, y_i) and (x_d, y_d) are the co-ordinates of sample, white light and dominant wavelength. The CIEL*a*b* color space diagram with L*a*b* parameters are shown below (Fig. 6b and Table 2). The L* represent the color coordinate of the sample on black-white (0 to 100) axis, a* on green-red axis (−60 to +60) and b* on blue-yellow (−60 to +60) axis. The difference in color is calculated by

$$\Delta E = (\Delta L^{*2} + \Delta a^{*2} + \Delta b^{*2})^{1/2}, \qquad (4)$$

where ΔL*, Δa*, and Δb*are the respective deviation of test with reference positions [21]. The cylindrical coordinates C^* (saturation) and h^* (hue angle or arctang) calculated by

$$h^* = \frac{a^*}{b^*}, \qquad (5)$$

$$C^* = (a^{*2} + b^{*2})^{1/2}. \qquad (6)$$

The L* value is near white light and ΔE* value is small, giving a fruitful output. So, from the CIE diagram and CIEL*a*b* color space parameters, it is clearly evident that $La_{1.97}Dy_{0.02}Sm_{0.01}MgTiO_6$ phosphor emit light identical to neutral daylight. That is, when the phosphor probe illuminates internal tissues, they resemble daylight exposure. Thus, the real-time recorded images appear precise and accurate. This in turn enhance the early detection and prevention of diseases. So $La_{1.97}Dy_{0.02}Sm_{0.01}MgTiO_6$ perovskite nano-phosphors brings out a new era of endoscope LEDs, which can improve human health sector, augment total well-being and develop holistic growth.

4 Conclusion

Biomedical engineering is striving hard to replace conventional imaging light sources with an environmentally friendly, flexible, energy-saving, efficient, and miniature arrangement, that could improve the accuracy of real-time recorded data. Double perovskites with variable formulas, flexible properties, and suitable optical bandgap, are the most suited candidates for such illumination devices. Sm^{3+} activated (x= 0%, 1%, 2%) $La_{1.98}Dy_{0.02}MgTiO_6$ is synthesized by combustion method. The crystal structure, morphology, size and phase are established by XRD, SEM, and TEM. With reference to concentration quenching, the co-doping concentration is optimized as 1%. PL studies show that the phosphor emits violet-blue-yellow-red wavelengths, with intensity 3-fold than conventional lighting sources, owing to $Dy^{3+}\rightarrow Sm^{3+}$ energy transfer mechanism of 53%. The CIE coordinates are (0.322, 0.324) with CCT being 5835 K, neighboring ideal white light; confirmed by CIEL**a***b** color space parameters. So, a meticulous optimization on broad white emission of $La_{1.97}Dy_{0.02}Sm_{0.01}MgTiO_6$ to the neutral point for biomedical application yield an accurate light source for endoscopic and laparoscopic applications.

Disclosures

The authors declare no conflict of interest.

Acknowledgment

Sincerely thanking Kannur University for providing all the necessary facilities during the course of the work.

References

1. K. Jorgenson, A. Alekseyko, and V. Giedraitis, "Energy consumption, human well-being and economic development in central and eastern European nations: A cautionary tale of sustainability," Energy Policy 66, 419–427 (2014).
2. S. D. Perli, N. Ahmed, and D. Katabi, "PixNet: Interference-free wireless links using LCD-camera pairs," Proceedings of the Sixteenth Annual International Conference on Mobile Computing and Networking, 137–148 (2010).
3. M. Pal Uttam, "Use of LED's in Endoscopy and Laparoscopy," LED inside of TRENDFORCE, 2014 (accessed 15 September 2022). [https://www.ledinside.com/knowledge/2014/2/use_of_leds_in_endoscopy_and_laparoscopy].
4. I. V. Ivanov, T. Mappes, P. Schaupp, C. Lappe, and S. Wahl, "Ultraviolet radiation oxidative stress affects eye health," Journal of Biophotonics 11(7), e201700377 (2018).
5. N. T. Clancy, R. Li, K. Rogers, P. Driscoll, P. Excel, R. Yandle, G. Hanna, N. Copner, and D. S. Elson, "Development and evaluation of a light-emitting diode endoscopic light source," Proceedings of SPIE 8214, 82140R (2012).
6. D. G. Adler, B. Chand, J. D. Conway, D. L. Diehl, S. V. Kantsevoy, R. S. Kwon, P. Mamula, S. A. Rodriguez, R. J. Shah, L. M. W. K. Song, and W. M. Tierney, "Capsule endoscopy of the colon," Gastrointestinal Endoscopy 68(4), 621–623 (2008).
7. V. P. Veena, C. K. Shilpa, S. V. Jasira, and K. M. Nissamudeen, "Modern era of double perovskite nano-phosphors: La2MgTiO6, Gd2MgTiO6 and Y2MgTiO6 – a brief review," Zeitschrift für Naturforschung A 77(10), 1003–1013 (2022).
8. V. P. Veena, C. K. Shilpa, S. V. Jasira, K. Vini, and K. M. Nissamudeen, "Adroit low-temperature synthesis and origin of blue–yellow–red emission in activated La2-xDyxMgTiO6 novel perovskite phosphor for WLED," Journal of Materials Science: Materials in Electronics 34, 870 (2023).
9. V. P. Veena, N. Akshaya, C. K. Shilpa, S. V. Jasira, and K. M. Nissamudeen, "The upshot of Li+ co-doping on white emission of La1.98Dy0.02MgTiO6 double perovskite nano phosphors," Materials Today: Proceedings (2023).
10. V. P. Veena, C. K. Shilpa, S. V. Jasira, and K. M. Nissamudeen, "Anti-Counterfeiting and Multifunctional Applications of Near White Emitting La1.99mgtio6:0.01dy Perovskite Nano Phosphors," Social Science Research Network (2023).
11. B. Bondzior, D. Stefańska, T. H. Q. Vũ, N. Miniajluk-Gaweł, and P. J. Dereń, "Red luminescence with controlled rise time in La2MgTiO6: Eu3+," Journal of Alloys and Compounds 852, 157074 (2021).
12. K. Vini, K. M. Nissamudeen, "Facile Combustion Synthesis of (Y, Pr) 2O3 Red Phosphor: Study of Luminescence Dependence on Dopant Concentration and Enhancement by the Effect of Co-dopant," Zeitschrift für Naturforschung A 75(4), 357–371 (2020).
13. M. Pal, U. Pal, J. M. G. Y. Jiménez, and F. Pérez-Rodríguez, "Effects of crystallization and dopant concentration on the emission behavior of TiO2: Eu nanophosphors," Nanoscale Research Letters 7, 1 (2012).
14. G. Tiwari, N. Brahme, R. Sharma, D. P. Bisen, S. K. Sao, and S. Tigga, "Luminescence properties of dysprosium doped di-calcium di-aluminium silicate phosphors," Optical Materials 58, 234–242 (2016).
15. W. Li, G. Fang, Y. Wang, Z. You, J. Li, Z. Zhu, C. Tu, Y. Xu, and W. Jie, "Luminescent properties of Dy3+ activated LaMgAl11O19 yellow emitting phosphors for application in white-LEDs," Vacuum 188, 110215 (2021).
16. I. P. Sahu, P. Chandrakar, R. N. Baghel, D. P. Bisen, N. Brahme, and R. K. Tamrakar, "Luminescence properties of dysprosium doped calcium magnesium silicate phosphor by solid state reaction method," Journal of Alloys and Compounds 649, 1329–1338 (2015).

17. I. P. Sahu, D. P. Bisen, N. Brahme, R. K. Tamrakar, and R. Shrivastava, "Luminescence studies of dysprosium doped strontium aluminate white light emitting phosphor by combustion route," Journal of Materials Science: Materials in Electronics 26, 8824–8839 (2015).
18. W. Yan, J. Li, W. Zhang, X. Gao, and P. Zhang, "Warm-white luminescence of Dy3+ and Sm3+ co-doped NaSrPO4 phosphors through energy transfer between rare earth ions," Journal of Materials Science: Materials in Electronics 32, 16648–16661 (2021).
19. H. Pamuluri, M. Rathaiah, K. Linganna, C. K. Jayasankar, V. Lavin, and V. Venkatramu, "Role of Dy3+ → Sm3+ energy transfer in the tuning of warm to cold white light emission in Dy3+/Sm3+ co-doped Lu3Ga5O12 nano-garnets," New Journal of Chemistry 42(2), 1260–1270 (2018).
20. M. Yu, X. Xu, W. Zhang, X. Chen, P. Zhang, and Y. Huang, "The effect of Sm3+ co-doping on the luminescence properties of Ca2.85Li0.15(PO4)1.85(SO4)0.15: Dy3+ white-emitting phosphors," Journal of Alloys and Compounds 817, 152761 (2020).
21. M. M. Gonzalez-Pena, M. D. Hale, "Colour in thermally modified wood of beech, Norway spruce and Scots pine. Part 1: Colour evolution and colour changes," 63(4), 385–393 (2009).